

# Cyclic Behavior of Asphalt Concrete Used as Impervious Core in Embankment Dams

Weibiao Wang<sup>1</sup> and Kaare Höeg, M.ASCE<sup>2</sup>

**Abstract:** Asphalt concrete is used as a water barrier (interior core or upstream facing) in embankment dams. This paper investigates the behavior of hydraulic asphalt specimens subjected to cyclic loading in a triaxial cell. The specimens were tested at various sustained static stress states and temperatures and at maximum cyclic shear stress levels corresponding to severe earthquake shaking of the dam. The cyclic modulus versus mean sustained static stress showed an approximately linear relationship in a logarithmic diagram, and an empirical expression was developed to determine the cyclic modulus. At a mean sustained stress of 1.0 MPa, the cyclic modulus at 20°C was about 900 MPa; at 9°C, it was 1900 MPa and at 3.5°C, about 2500 MPa. The damping ratio was found to be between 0.07–0.30, depending on stress state and temperature level. The number of load cycles (up to 6000) had no significant effect on the magnitude of cyclic strain, and the cyclic loading was documented to have little effect on the postcyclic monotonic stress-strain-strength behavior and permeability (watertightness) of the asphalt concrete. DOI: 10.1061/(ASCE)GT.1943-5606.0000449. © 2011 American Society of Civil Engineers.

**CE Database subject headings:** Dams, embankment; Asphalts; Concrete; Earthquake resistant structures; Cyclic loads; Permeability.

**Author keywords:** Embankment dams; Dam core; Asphalt concrete; Earthquake resistance; Cyclic loading; Cyclic degradation; Postcyclic behavior; Permeability.

## Introduction

The first embankment dam with a compacted asphalt concrete core was built in Germany in 1961–1962. Hydropower and Dams (2009) provides an overview of asphalt core dams that have been built or are currently under construction in different countries. Several dams have been extensively instrumented and monitored to document the dam performance and design assumptions (e.g., Breth 1964; Penman and Charles 1985; Pircher and Schwab 1988; Arnevik et al. 1988; Tschernutter 1997; Strobl and Schmid 1993; Höeg et al. 2007). The International Commission on Large Dams (ICOLD) and others have summarized the experience with the design, construction, and performance of this type of dam (e.g., ICOLD 1992; Höeg 1993; Creegan and Monismith 1996; Schönián 1999). Wang (2008) presented experimental and field results and discussed the ductility, cracking resistance, permeability, and viscoelastic-plastic properties of asphalt concrete used in hydraulic structures.

For a given embankment dam project site, there are several different design options; e.g., a dam with (1) earth core; (2) upstream facing of reinforced concrete or asphalt or synthetic geomembrane; or (3) asphalt core. Höeg et al. (2007) presented the field performance observations for the Storglomvatn asphalt concrete core dam (125 m high; Fig. 1) and provided a general discussion of the

relative merits of the different embankment dam design options. Comparative studies at several recent projects have shown the asphalt concrete core option to be very competitive both technically and economically. The increased use of asphalt concrete rather than earth core is partly due to the profession's increased concern about internal erosion of earth cores. An asphalt concrete core is erosion-resistant and does not require a filter for erosion protection. Furthermore, the core may be constructed in cold and rainy weather without construction delays.

Typically, the central or sloped asphalt concrete core wall may be between 0.5 and 1.0 m wide, depending on the height of the dam, seismicity of the site, foundation conditions, and quality of the embankment fill. Inside the embankment, the asphalt concrete is protected from the environment and is subjected to almost constant temperature after the end of dam construction and reservoir impounding. Thus, weathering and aging are of little concern.

The slender core wall has to adjust to the deformations of the embankment fill during construction, impounding, operation, and earthquake-loading. The quality control of the asphalt mix and material properties is relatively simple to carry out in the field laboratory and during field construction. The asphalt concrete can be made virtually impervious and flexible, with ductile stress-strain behavior that offers jointless core construction as the hot asphalt concrete is being compacted in 0.2–0.3-m-thick horizontal layers (Fig. 1(c)). The viscoelastic-plastic properties provide a self-healing (self-sealing) ability, should any cracks develop, for instance, as a result of earthquake-loading. Kramer (1988) reported that “the rockfill dam with an asphalt-diaphragm is an appropriate dam type for the very highest future dams.”

Several dams of this type are currently under construction in China. The recently built 125-m-high Yele Dam is founded on a deep and complex alluvial foundation in a high intensity seismic region (Wang 2008). Based on their experience, Chinese engineers have now designed and are building a 170-m-high asphalt concrete core rockfill dam (Quxue dam). Canada has recently completed an asphalt concrete core dam (Alicescu et al. 2008), the first of its kind

<sup>1</sup>Associate Professor, Dept. of Hydraulic Engineering, Xi'an Univ. of Technology, 5 Jinhua South Road, 710048 Xi'an, China (corresponding author). E-mail: wangweibiao59@hotmail.com

<sup>2</sup>Professor, Dept. of Geosciences, Univ. of Oslo; and Special Adviser, Norwegian Geotechnical Institute, P.O. Box 3930, Ullevaal Stadion, NO-0806 Oslo, Norway. E-mail: kh@ngi.no

Note. This manuscript was submitted on February 9, 2009; approved on September 22, 2010; published online on September 24, 2010. Discussion period open until October 1, 2011; separate discussions must be submitted for individual papers. This paper is part of the *Journal of Geotechnical and Geoenvironmental Engineering*, Vol. 137, No. 5, May 1, 2011. ©ASCE, ISSN 1090-0241/2011/5-536–544/\$25.00.

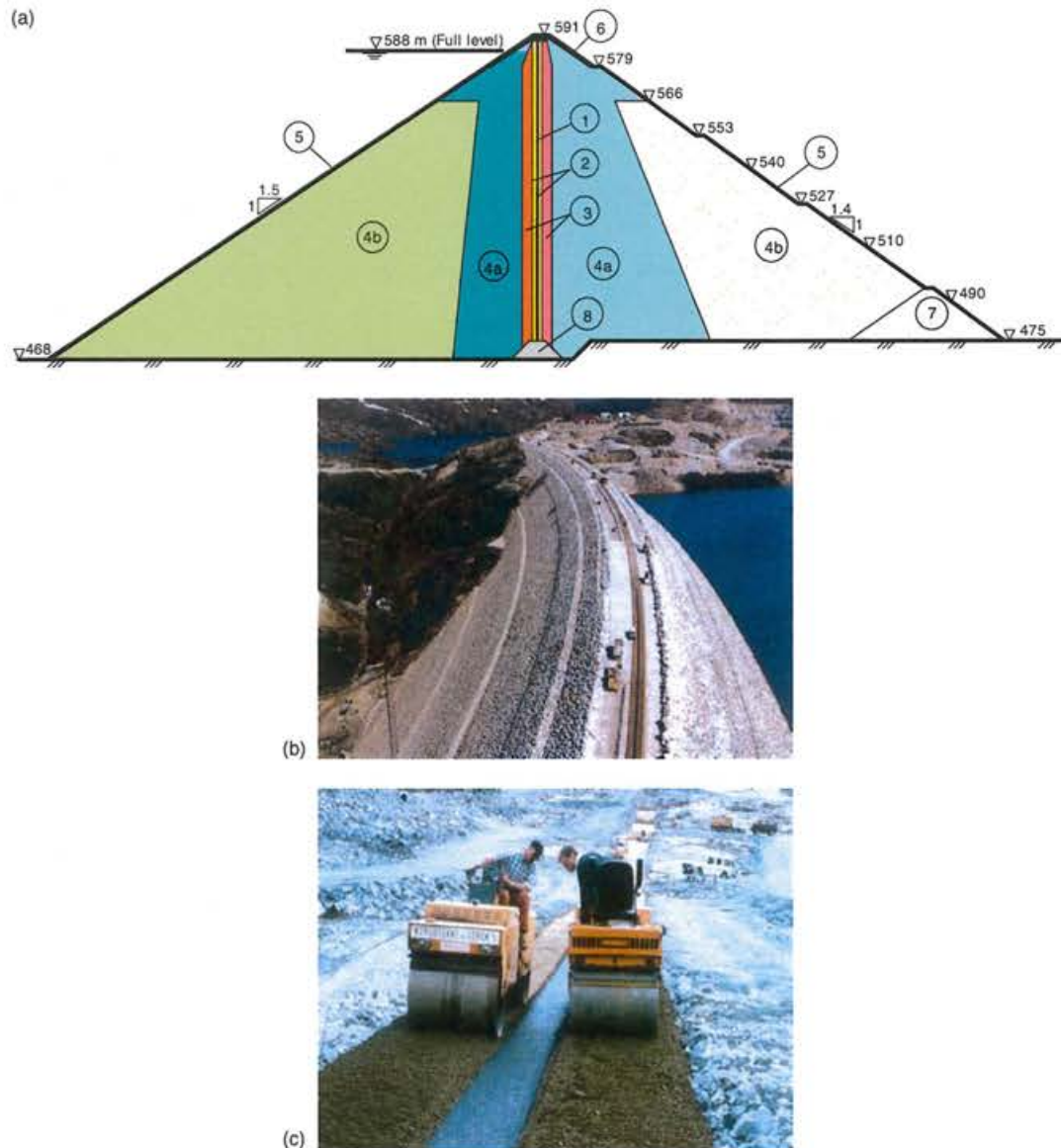


**Fig. 1.** Design and construction of Storglomvatn Dam, Norway (125 m high) with asphalt concrete core (Höeg et al. 2007, with permission from *Int. Journal on Hydropower and Dams*): (a) Zoning of asphalt concrete core rockfill dam; (1) = asphalt core; (2) = transition zone of gravel (0–60 mm); (3) = transition zone of crushed rock (0–150 mm); (4a) = well-compacted quarried rock (0–700 mm); (4b) = shoulder of quarried rock (0–1000 mm); (5) = rip rap; (6) = crown cap protection (blocks > 1 m<sup>3</sup>); (7) = toe drain (blocks > 0.5 m<sup>3</sup>); (8) = concrete plinth; (b) construction nearing completion, showing central core and transition zone #2; (c) simultaneous placement and compaction of asphalt core with transition zones

in North America, and Hydro Québec has decided to build several more embankment dams of this type in the Province of Quebec. Brazil is currently building its first asphalt concrete core dam (Foz do Chapeco).

There is a significant amount of laboratory and field research on hydraulic asphalt reported in the literature. However, there are only a few experimental studies performed to investigate the behavior of hydraulic asphalt concrete subjected to cyclic loads simulating earthquake shaking. Breth and Schwab (1973) performed a cyclic direct shear test on an asphalt concrete specimen simulating an element of the core inside an embankment dam. Though the test was not continued beyond the preliminary stage, they concluded that the imposed cyclic loading had no significant degradation effects. That was the state of the art until Nakamura et al. (2004)

performed cyclic tension tests on asphalt concrete specimens to simulate the tension conditions that may arise in the upstream facing of a dam subjected to seismic loads. They also studied the use of an additive in the asphalt concrete mix to increase ductility and resistance to cracking. Recently, Feizi-Khankandi et al. (2008) reported the results of cyclic triaxial tests to derive material parameters for the seismic analysis of the Garmrood asphalt concrete core embankment dam in northern Iran.

The purpose of this paper is to systematically study the effects of cyclic loading on the stress-strain-strength behavior and permeability of asphalt concrete at different temperatures and static and cyclic stress conditions. The effects of a large number of load cycles, much larger than the number of significant cycles in an earthquake, were also studied. The postcyclic stress-strain-strength behavior

and permeability are compared with that of specimens not subjected to prior cyclic loading to study any degradation/deterioration effects caused by the cyclic loading.

### Mix Design of Asphalt Concrete for Dam Cores

The mix design of asphalt concrete used in impervious facings and cores in embankment dams originated from road asphalt concrete experience. However, there are significant differences between a road pavement and an interior dam core with respect to loading and environmental conditions. Typically, road asphalt concrete mixes consist of 4–6% bitumen (asphalt cement) by mineral weight, 4–8% filler material (< 0.075 mm), and 20–40% fine aggregates (0.075–2.36 mm). The air voids content for road asphalt concrete after compaction is in the range 3–10%.

The asphalt concrete used in dams and canals (hydraulic asphalt concrete) is required to be impervious and flexible and it consists of more fine aggregates, filler and bitumen than the asphalt concrete used in pavements. Typically, asphalt concrete for impervious cores consists of 6.5–8.5% bitumen by mineral weight, 10–15% filler material (< 0.075 mm), 35–52% fine aggregates (0.075–2.36 mm), and 33–55% coarse aggregates (2.36–19 mm, square mesh sieve). In core construction, 0.2–0.3-m-thick asphalt concrete layers are compacted by a 0.5–1.0 ton vibratory roller to meet the required air voids content of a maximum of 3% which gives a virtually impervious asphalt concrete. Field measurements often show values in the range 1.0–2.5% (e.g., Saxegaard 2002).

Table 1 shows the asphalt concrete mixes used for three asphalt concrete core embankment dams located in seismic regions in China—the Longtoushi Dam in Sichuan Province, and the Xiabandi Dam and Qiapuqihai Dam in Xinjiang Uygur Autonomous Region. The asphalt concrete mixes and material properties for the three cores are not identical but are very similar. The coarse aggregates were crushed limestone, natural gravels, and river sand, giving a grain-size distribution satisfying the Fuller curve (Höeg 1993). About 13% of limestone filler was added to the aggregates in all three mixes. The same bitumen type, B70, was used, 6.9% (by aggregate mineral weight) for the Longtoushi and Qiapuqihai dams, and 7.2% for the Xiabandi Dam, because the Xiabandi aggregates absorbed a little bitumen.

### Results of Triaxial Tests with Cyclic Loading

#### Testing Conditions

The compacted triaxial specimens were 100 mm in diameter and 200 mm high. They were prepared using a compaction method simulating the field roller compaction of the core (Wang and Höeg 2009). The air voids content was between 0.9 and 2.3% for the

prepared specimens. The volumetric properties of the asphalt concrete specimens are shown in Table 1 (right columns).

The testing temperatures used were the local annual average temperatures at the three project sites—3.5°C at Xiabandi, 9°C at Qiapuqihai, and 20°C at Longtoushi. Tests were also carried out at 20°C for the Qiapuqihai specimens to compare behavior at different temperatures.

As the mix design and application conditions are significantly different between road asphalt concrete and hydraulic asphalt concrete used in impervious facings and cores in embankment dams, the corresponding methodology to study the hydraulic asphalt concrete behaviors has been investigated in China since the 1970s. In 2006, China issued the Test Code for Hydraulic Bitumen Concrete (DL/T 5362-2006). The tests discussed subsequently were run according to the test code for the study of cyclic loading modulus and damping ratio.

Fig. 2 shows the cyclic loading test equipment. Radial confining stress and axial stress were imposed in small simultaneous steps on the specimen until the specified initial static stress state was reached. Then, the cyclic axial loading (sinusoidal) was applied with a frequency of 1 Hz. The equipment may also be used to determine Poisson's ratio by measuring the volume change of the specimen during cyclic loading. The volume change is measured by adjusting the water level to be close to the tactile needle point by moving the piston of the volumetric gauge.

Prior to cyclic loading, the initial (sustained) static stresses were applied with the stress ratio  $K_c = \sigma_1/\sigma_3$ . In each cyclic test, the confining stress ( $\sigma_3$ ) was kept constant, and cyclic loading was only applied in the axial direction. The cyclic axial stress was increased in steps, and five stress cycles were applied at each level of cyclic stress.

The level of imposed cyclic stress, simulating realistic field conditions for embankment dams in earthquake regions, was based on the results of numerical analyses. Ghanooni and Mahin-roosta (2002) performed two-dimensional dynamic analyses for a typical 115-m-high asphalt concrete core rockfill dam on a rock foundation. They input a strong earthquake with a peak horizontal ground acceleration of 0.54 g and computed a maximum induced tensile stress of 0.18 MPa in the top part of the asphalt core and a maximum induced cyclic shear stress of 0.7 MPa toward the base of the core. Feizi-Khankandi et al. (2009) performed two-dimensional dynamic analyses for the 110-m-high Garmrood asphalt core rockfill dam, with a horizontal peak ground acceleration of 0.54 g. They computed a maximum tensile stress of 0.20 MPa and a maximum cyclic shear stress of 1.0 MPa in the asphalt core. Three-dimensional dynamic analyses for the Yele asphalt core rockfill dam were performed with a horizontal peak ground acceleration of 0.45 g, and the computed maximum tensile stress and maximum cyclic shear stress in the asphalt concrete core were 0.55 MPa and 0.5 MPa, respectively (CHIDI 2006). Chen et al. (2008) recently performed three-dimensional dynamic design analyses for the

**Table 1.** Mixes of Three Asphalt Concrete Cores (% of Aggregate Mineral Weight) and Volumetric Properties of Asphalt Concrete Specimens

Dam name	Sieve size (mm)					Bitumen content(%)	Asphalt concrete triaxial specimens		
	Crushed aggregates			River sands < 2.36	Filler < 0.075		Air voids (%)	VMA (%)	VFB (%)
	9.5–19	2.36–9.5	< 2.36						
Xiabandi	22.2	30.8	17.0	17.0	13	7.2	1.6–2.3	18.0–18.6	91.1–87.6
Longtoush	23.3	30.7	16.0	16.0	14	6.9	1.5–2.1	17.7–18.2	91.5–88.5
Qiapuqihai	22.6	30.8	16.4	16.4	13.8	6.9	0.9–1.3	16.8–17.1	94.6–92.6

Note: VMA = volume of air and bitumen in percentage of total volume of specimen; VFB = volume of bitumen in percentage of volume of air and bitumen.

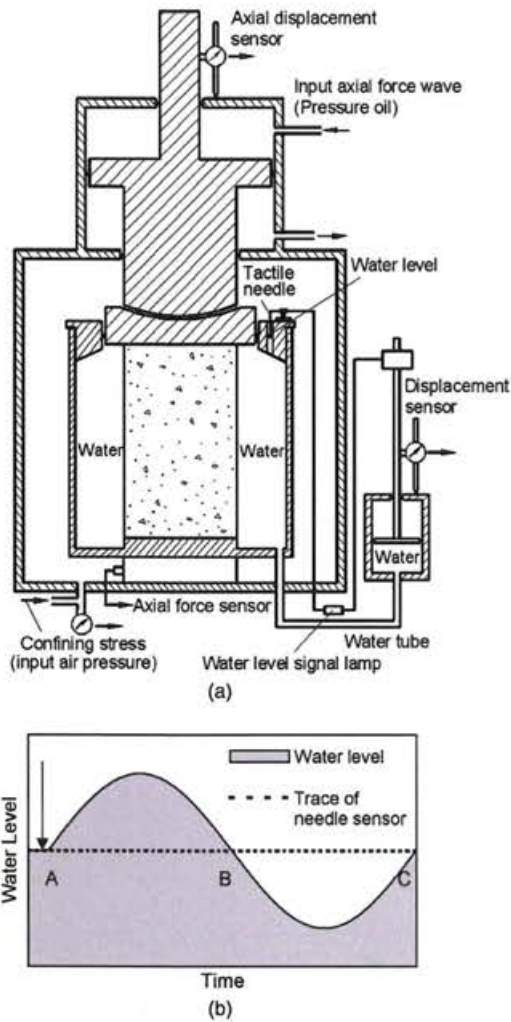


Fig. 2. (a) Triaxial equipment developed for cyclic axial loading of asphalt concrete; (b) trace of needle point and water level when running cyclic loading

Quxue asphalt concrete core rockfill dam with a height of 170 m and crest length of 219 m in a fairly narrow gorge. They input an earthquake with a horizontal peak ground acceleration of 0.23 g and computed a maximum tensile stress of 0.54 MPa and a maximum cyclic shear stress of 0.4 MPa in the core. All the investigators concluded that the computed dynamic tensile stresses are much lower than the tensile strength of asphalt concrete determined in dynamic tension tests with high strain rates.

### Triaxial Test Results

For the cyclic triaxial tests, the half-amplitude of the imposed cyclic stress is denoted by  $\sigma_d$ , and the corresponding half-amplitude of the cyclic strain is denoted by  $\varepsilon_d$ . Under a small initial static deviator stress (e.g.,  $\sigma_3 = 500$  kPa,  $K_c = 1.2$ ) and relatively small cyclic axial stress (e.g.,  $\sigma_d = 270$  kPa), the resulting axial strain was virtually elastic and the residual strain negligible. Under a larger initial deviator stress (e.g.,  $\sigma_3 = 500$  kPa,  $K_c = 2.0$ ) and larger cyclic loading stress (e.g.,  $\sigma_d = 550$  kPa), the resulting axial cyclic strain was still approximately constant, but there was also some residual strain. However, creep tests demonstrated that the residual strain was mainly caused by the sustained static deviator stress and

not by degradation caused by the cyclic loading (Wang 2008). If the cyclic stress  $\sigma_d$  is more than the specified static axial stress  $\sigma_1$ , the resulting axial stress will be in tension. That was not experimentally possible with the triaxial equipment used. Therefore, the available maximum cyclic loading stress  $\sigma_d$  was always specified to be smaller than the specified sustained axial stress  $\sigma_1$ , i.e., one-way axial loading. However, the maximum cyclic shear stress in the specimen will reverse direction during the cyclic loading (two-way cyclic shearing), as is the case, for example, for a horizontal element in an asphalt core during earthquake shaking.

Fig. 3 shows a typical cyclic stress-strain hysteresis loop for a test. The cyclic modulus ( $E_d$ ) is calculated as

$$E_d = \frac{\sigma_d}{\varepsilon_d} \quad (1)$$

The damping ratio ( $\lambda_d$ ) is calculated as

$$\lambda_d = \frac{1}{4\pi} \frac{S}{S_{\Delta}} \quad (2)$$

where  $S$  = area of the hysteresis loop in a single loading cycle; and  $S_{\Delta}$  = area of the triangle OAE in Fig. 3.

The shape and area of the cyclic stress-strain hysteresis loop depends on the level of sustained static stress state, temperature, and magnitude of imposed cyclic stress on a given asphalt concrete mix. For a low static stress state and at high temperature, the cyclic modulus on the extension side is somewhat lower than that on the compression side. Fig. 3 shows such an example in which the static confining stress was 500 kPa, and the stress ratio was 1.2 at 20°C. For higher static stresses, the extension cyclic modulus and compression cyclic modulus were nearly identical. This agrees with the findings of Feizi-Khankandi et al. (2008). In the subsequent presentation and discussion of results, the cyclic modulus ( $E_d$ ) is taken as the average value of extension and compression cyclic modulus determined from the cyclic stress-strain hysteresis loops.

Imposed cyclic stress ( $\sigma_d$ ) versus resulting cyclic strain ( $\varepsilon_d$ ) for the three asphalt concrete materials (Table 1) at different sustained static stress states and temperature conditions are shown in Figs. 4–7. The damping ratio computed from the hysteresis curves is also shown in the figures. The figures show that, for all the static and cyclic stress combinations and temperature conditions, the cyclic stress  $\sigma_d$  versus cyclic strain  $\varepsilon_d$  gives an almost linear relationship. It is only when the imposed  $\sigma_d$  is approaching the sustained static stress  $\sigma_1$  that the  $\sigma_d$  versus  $\varepsilon_d$  diagrams show a tendency to deviate from a straight line. Under all the different stress states and temperature conditions tested, the maximum cyclic strain was less than 0.3%, although high static deviator stress and cyclic stress levels were applied, corresponding to severe earthquake loading of the dam (e.g., Ghanooni and Mahin-roosta 2002).

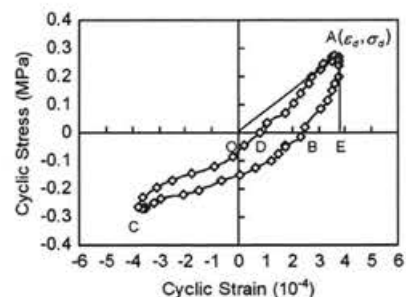
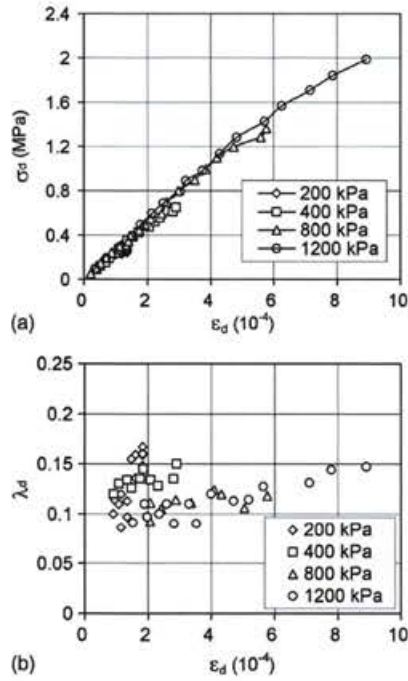
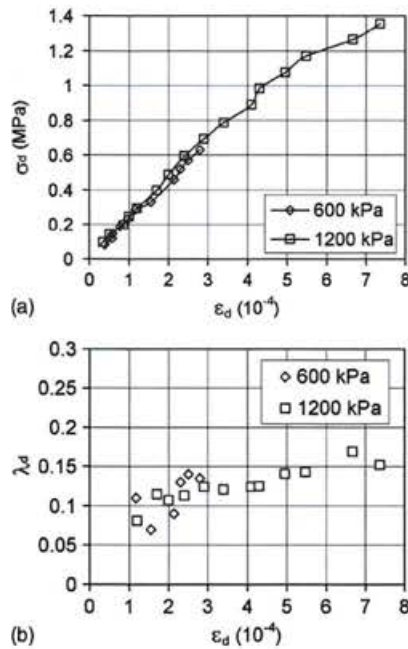


Fig. 3. Typical cyclic stress-strain hysteresis loop



**Fig. 4.** (a) Cyclic stress versus cyclic strain; (b) damping ratio versus cyclic strain at  $K_c = 1.8$  for different values of confining stress for Xiabandi asphalt concrete specimens at 3.5°C

Figs. 4–7 show that the computed damping ratios were between 0.07 and 0.23. Figs. 4 and 5 show that the damping ratio increased somewhat with cyclic strain level. On the other hand, Figs. 6 and 7 show a reduction in damping ratio with increasing cyclic strain. Considering all the tests performed in the study, one found the damping ratio to lie between 0.07 and 0.30, depending on the stress



**Fig. 5.** (a) Cyclic stress versus cyclic strain; (b) damping ratio versus cyclic strain at  $K_c = 1.2$  for different values of confining stress for Qiapuqihai asphalt concrete specimens at 9°C

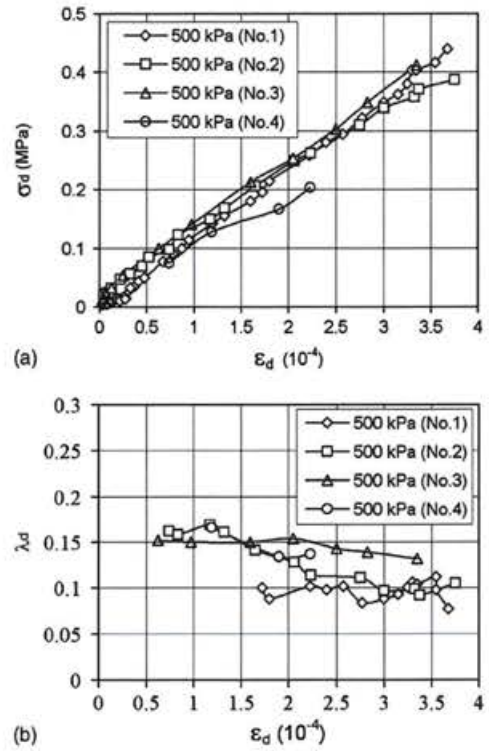


**Fig. 6.** (a) Cyclic stress versus cyclic strain; (b) damping ratio versus cyclic strain for confining stress of 500 kPa and  $K_c = 2.0$  for Qiapuqihai asphalt concrete specimens at 20°C (four specimens at same confining stress)

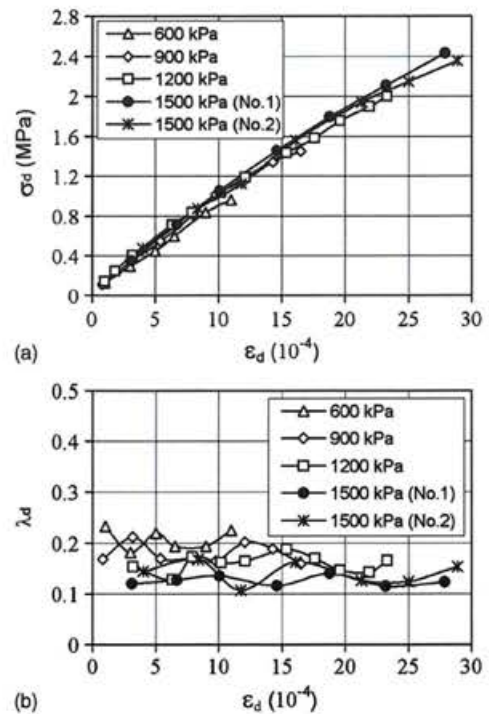


**Fig. 7.** (a) Cyclic stress versus cyclic strain; (b) damping ratio versus cyclic strain at  $K_c = 1.8$  for different values of confining stress for Longtoushi asphalt concrete specimens at 20°C

**Table 2.** Static and Cyclic Test Conditions and Resulting Cyclic Modulus

Dam name	Temp. (°C)	$K_c (\sigma_1/\sigma_3)$	$\sigma_3$ (kPa)	$E_d$ (MPa)	$K_c (\sigma_1/\sigma_3)$	$\sigma_3$ (kPa)	$E_d$ (MPa)	
Xiabandi	3.5	1.2	200	2,000	1.8	200	2,100	
			400	2,200		400	2,300	
			800	2,800		800	2,600	
			1,200	2,300		1,200	2,800	
Qiapuqihai	9	1.2	600	2,200	1.5	800	1,700	
			1,200	1,900		1,200	2,100	
		1.5	200	1,100	1.8	600	1,700	
			400	1,500				
	20	1.2	600	1,200		1,200	2,400	
			500	730	1.0	1,000	940	
		1.5		730	1.2		810	
				1,100	1.5		1,000	
Longtoushi	20	1.2	900	800	1.8	600	900	
			1,200	900		900	1,100	
				950			1,200	1,100

state and the temperature level. This range agrees very well with that obtained by Feizi-Khankandi et al. (2008).

A summary of all the test conditions and test results is given in Table 2, which shows that, for the Xiabandi Dam asphalt concrete specimens tested at 3.5°C, the cyclic loading modulus is very high, between 2,000 and 2,800 MPa. For the Qiapuqihai Dam specimens at 9°C, the modulus is between 1,100 and 2,400 MPa, and for the Qiapuqihai and Longtoushi Dam specimens at 20°C, the modulus is between 730 and 1,100 MPa.

If the cyclic modulus  $E_d$  is plotted versus mean stress  $\sigma_m$  in a logarithmic diagram, as shown in Fig. 8, the test results show an almost linear relationship. The expression is

$$E_d = kp_a \left( \frac{\sigma_m}{p_a} \right)^n \quad (3)$$

where  $\sigma_m$  = mean sustained stress,  $\sigma_m = (\sigma_1 + 2\sigma_3)/3$  MPa;  $p_a$  = atmospheric pressure—0.1 MPa (a reference stress level); and  $k, n$  = test parameters determined by regression analysis of the experimental data (see values in Fig. 8).

Table 2 and Fig. 8 show that temperature has a very significant effect on the cyclic modulus. At a mean sustained stress of 1.0 MPa,

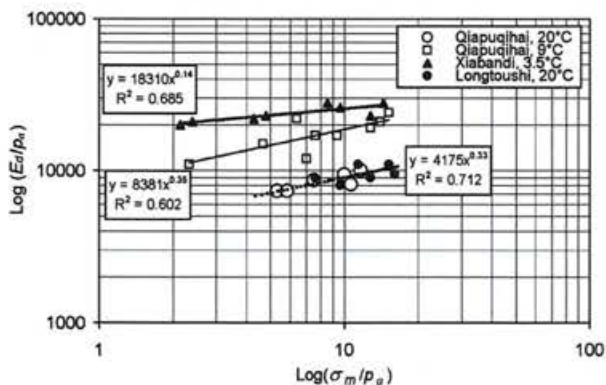


**Fig. 8.**  $\log(E_d/p_a)$  versus  $\log(\sigma_m/p_a)$  for three asphalt concrete core materials at 3.5°C, 9°C, and 20°C, respectively. In equations shown in figure,  $y = E_d/p_a$  and  $x = \sigma_m/p_a$

the cyclic loading modulus at 20°C is about 900 MPa, at 9°C, about 1900 MPa, and at 3.5°C, about 2500 MPa. Fig. 8 also shows that the cyclic moduli at 20°C for the Qiapuqihai and Longtoushi asphalt concrete specimens agree quite well with each other. The cyclic modulus was also investigated using Qiapuqihai asphalt concrete specimens with a somewhat lower bitumen content, tested at 9°C. The test results show that a 0.3% decrease in bitumen content from 6.9% to 6.6% did not give any significant difference in the cyclic modulus.

During the cyclic triaxial tests, the specimen volume change was measured, and Poisson's ratio could be computed. The computed Poisson's ratio during cyclic loading was found to be between 0.31 and 0.38, with an average of 0.35 for all the specimens.

### Effects of Many Loading Cycles

In the tests described in the preceding sections, 5 load cycles were applied at each cyclic stress level. Only very small residual strains were recorded after the five cycles of loading. In a supplementary series of tests, a large number of cycles were imposed on Qiapuqihai specimens at various stress states and at 9°C.

Prior to cyclic loading, the specimens were first allowed to creep for 40 min under the sustained static stress condition. Significant creep occurred, but the period was not long enough to reach a fully "creep stable state," as discussed by Wang (2008). Then, the cyclic

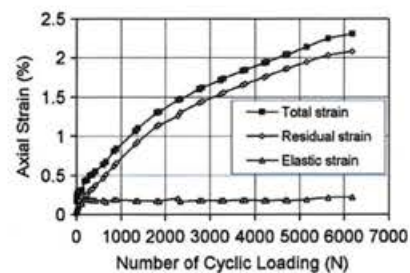


**Fig. 9.** Axial strain versus number of load cycles for confining stress 1.2 MPa and  $K_c = 1.5$  at 9°C for Qiapuqihai specimen with bitumen content 6.6% and  $\sigma_d = 1.0$  MPa

**Table 3.** Specimen Parameters and Test Program

Specimen no.	Air voids (%)		Test item	
Q1	1.5		Permeability	
Q2	1.7	Allowed to creep for 5 hrs	Monotonic loading	
Q3	1.7			
Q4	1.9			
Q5	1.7	Allowed to creep for 5 hrs	Cyclic loading	Monotonic loading
Q6	1.6			
Q7	1.9			
Q8	2.0	Allowed to creep for 5 hrs	Cyclic loading	Permeability
Q9	2.0			
Q10	2.0			

loading was imposed, and the elastic and residual strains were measured. Typical results are shown in Fig. 9.

During more than 6,000 cycles of loading, the cyclic strain magnitude stayed constant. Even for this high cyclic stress of 1 MPa, the number of cycles had virtually no effect on the magnitude of cyclic strain. However, the residual strain increased with the number of cycles. The residual strain recorded is predominantly creep strain caused by the sustained static deviator stress, as shown by Wang (2008).

**Postcyclic Stress-Strain-Strength Behavior and Permeability**

When the specimens tested in the previous sections were dismounted from the triaxial cell after cyclic loading, there was no visible damage (fissures or cracks) observed in the specimens. To compare the postcyclic behavior of specimens subjected to cyclic loads to that of specimens that had not been subjected to cyclic loads, a special test series was run. Qiapuqihai asphalt concrete specimens with a bitumen content of 6.9% were tested at 9°C. The test program is shown in Table 3 and is explained subsequently.

**Permeability Reference Test on Unloaded Specimen**

Triaxial specimen Q1 was not subjected to any static or cyclic stress. The Q1 specimen, with a length of 200 mm, was cut into three disk specimens, each with height 63.5 mm, and tested in a permeameter with axial flow for two days (Wang 2008); coefficients of permeability lower than  $10^{-8}$  cm/s cannot be accurately measured in this permeameter. After one day, the measured coefficients of permeability of the three disk specimens were  $2.3 \times 10^{-8}$ ,  $2.7 \times 10^{-8}$  and  $< 10^{-8}$  cm/s. After two days of flow, all the measured coefficients were  $< 10^{-8}$  cm/s.

**Monotonic Loading of Specimens Not Previously Subjected to Cyclic Loading**

Asphalt specimens Q2–Q10, in Table 3, were all subjected to the same static sustained stress state with confining stress 1.0 MPa and axial stress 1.7 MPa for 5 h. The creep test results gave axial strains of the specimens of around 1.7% during this period. Then the three specimens Q2–Q4 were each subjected to monotonic axial compression loading (unconfined). The axial deformation rate was 1.0 mm/min. The average stress-strain-strength curve for the three specimens is shown in Fig. 10.

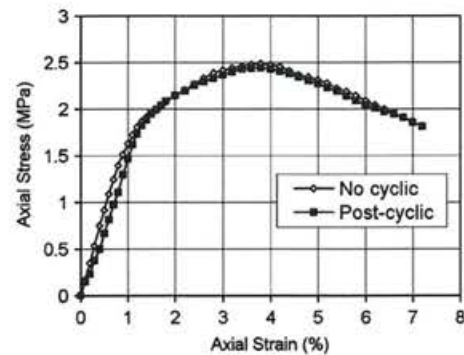


**Fig. 10.** Comparison of average unconfined postcyclic monotonic stress-strain-strength curve for specimens subjected to cyclic loading with average curve for specimens not subjected to cyclic loading

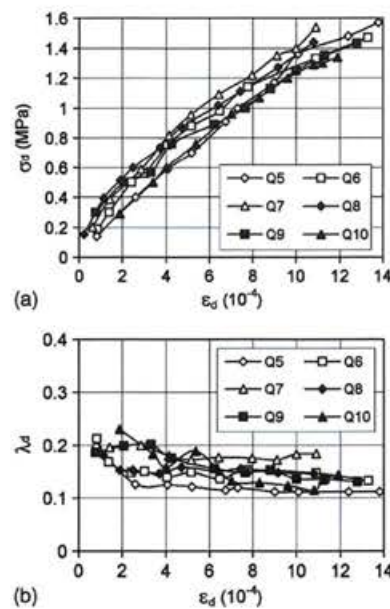


**Fig. 11.** (a) Cyclic stress versus cyclic strain; (b) damping ratio versus cyclic strain for specimens Q5–Q10

### Cyclic Loading Test

Cyclic loading tests were carried out on the six specimens Q5–Q10, shown in Table 3. The cyclic axial stress  $\sigma_d$  was increased, in 10 steps, up to 1.5 MPa, and at each stress level 30 load cycles with a frequency of 1 Hz were applied. The curves in Fig. 11 which show the cyclic stress and damping ratio versus cyclic strain for the six specimens, agree quite well. The recorded accumulated residual strains for all the specimens were around 0.6%.

### Monotonic Loading after Completed Cyclic Loading

The three specimens Q5–Q7, in Table 3, were dismantled from the triaxial cell after being subjected to the cyclic loading, and monotonic loading tests (unconfined) were carried out as for the three specimens Q2–Q4 which were not subjected to cyclic loading. The two average stress-strain-strength curves in Fig. 10 are almost identical and indicate that the cyclic loading has had virtually no degradation effect on the stress-strain-strength behavior of the asphalt concrete.

### Permeability of Specimens Subjected to Cyclic Loading

The three specimens Q8–Q10, shown in Table 3, were dismantled from the triaxial cell after being subjected to the cyclic loading. Each specimen was cut into three disk specimens, and permeability tests were performed as for specimen Q1 which had not been subjected to static and cyclic loading.

After having been subjected to the static and cyclic loading, specimens Q8–Q10 had a reduced air voids content compared to the initial air voids content, from the initial 2% to around 1.5%. The measured coefficients of permeability of the nine disk specimens from specimens Q8–Q10 were in a range of  $< 10^{-8}$  to  $5 \times 10^{-8}$  cm/s after one day and were all  $< 10^{-8}$  cm/s after two days of flow. The permeability test results show that the coefficient of permeability of the specimens subjected to the static and cyclic loading has not increased in spite of the high static deviator stress and cyclic stress levels imposed. Thus, no fissures or cracks can have opened.

### Summary and Conclusions

Cyclic loading with frequency 1 Hz was carried out on triaxial specimens of asphalt concrete at temperatures of 3.5°C, 9°C, and 20°C. The sustained lateral confining stresses were in the range 0.2–1.5 MPa, and the sustained static stress ratio (axial stress/radial stress) in the range 1.2–2.0. Imposed cyclic axial stress (half-amplitude) was up to 2.4 MPa, i.e., the maximum imposed cyclic shear stress was 1.2 MPa. Cyclic and residual strains were recorded for the different static and cyclic stress combinations and temperatures.

In a supplementary series of tests, the effects of the number of load cycles was investigated by using thousands of load cycles.

The postcyclic stress-strain-strength behavior and permeability were compared with that of specimens not subjected to previous cyclic loading to study any degradation/deterioration effects caused by the cyclic loading.

One may draw the following conclusions:

- The cyclic stress versus cyclic strain relationship was found to be nearly linear for all the conditions tested, although the cyclic shear stresses imposed on some of the specimens corresponded to severe earthquake shaking.
- The resulting cyclic strain was less than 0.3% in all tests, and the damping ratio was found to be between 0.07 and 0.30, depending on stress state and temperature level.

- The cyclic modulus versus mean static stress showed an approximately linear relationship in a logarithmic diagram, and an empirical expression was developed to determine the cyclic modulus,  $E_d$ , as shown in Eq. (3).
- The test temperature had a significant effect on the value of the cyclic modulus. As an example, at 1 MPa mean sustained stress, the cyclic modulus at 20°C was approximately 900 MPa, at 9°C, it was 1,900 MPa, and at 3.5°C, about 2,500 MPa.
- The number of load cycles (up to 6,000) had no significant effect on the magnitude of induced cyclic strain, but there was an accumulation of residual (plastic) strains, primarily due to creep under the sustained static stress on the specimens.
- The cyclic loading had very little degrading effect on the post-cyclic stress-strain-strength behavior and on the watertightness of the asphalt concrete.

The results show that the asphalt concrete core in an embankment dam in a seismic region can withstand very severe seismic shaking without cracking and losing watertightness. The earthquake resistance of the dam will depend on proper design and zoning of the embankment itself, considering the available fill materials, the foundation conditions, and the seismicity of the site.

### References

- Alicescu, V., Tournier, J. P., and Vannobel, P. (2008). "Design and construction of Nemiscau-1 Dam, the first asphalt core rockfill dam in North America." Proc., CDA 2008 Annual Conf., Canadian Dam Association.
- Arnevik, A., Kjaernsli, B., and Walbø, S. (1988). "The Storvatn Dam—a rockfill dam with a central core of asphaltic concrete." *Transactions, 16th Int. Congress on Large Dams*, R.9-Q.61, ICOLD Press, Paris, 141–158.
- Breth, H. (1964). "Measurements on a rockfill dam with bituminous concrete diaphragm." *Transactions, 8th Int. Congress on Large Dams*, R.17-Q.29, ICOLD Press, Paris, 305–315.
- Breth, H., and Schwab, H. (1973). "Stresses on asphaltic concrete cores in high dams during actual construction and during earthquakes." Strabag Publications, Series 9, Issue 1, 121–134. First published in *Die Wasserwirtschaft*, 1973, 63 Jahrgang, Heft 5–6, 194–197 (in German).
- Chen, Y., Li, S., and Wang, W. (2008). "Three-dimensional seismic analysis on Quxue asphalt core rockfill dam." Xi'an University of Technology, Xi'an, China.
- CHIDI. (2006). "Three-dimensional finite element back-analysis on Yele asphalt core rockfill dam and foundation." Chengdu Hydroelectric Investigation and Design Institute, Chengdu, China.
- Creegan, P. J., and Monismith, C. L. (1996). *Asphalt concrete water barriers for embankment dams*, ASCE Press, Reston, VA.
- Feizi-Khankandi, S., Ghalandarzadeh, A., Mirghasemi, A. A., and Höeg, K. (2009). "Seismic analysis of the Garmrood embankment dam with asphaltic concrete core." *Soils Found.*, 49(2), 153–166.
- Feizi-Khankandi, S., Mirghasemi, A. A., Ghalandarzadeh, A., and Höeg, K. (2008). "Cyclic triaxial tests on asphalt concrete as a water barrier for embankment dams." *Soils Found.*, 48(3), 319–332.
- Ghanooni, S., and Mahin-roosta, R. (2002). "Seismic analysis and design of asphaltic concrete core embankment dams." *Int. J. Hydropower Dams*, 9(6), 75–78.
- Höeg, K. (1993). *Asphaltic concrete cores for embankment dams*, Stikka Press, Oslo, Norway.
- Höeg, K., Valstad, T., Kjaernsli, B., and Ruud, A. M. (2007). "Asphalt core embankment dams: Recent case studies and research." *Int. J. Hydropower Dams*, 13(5), 112–119.
- Hydropower and Dams. (2009). "Asphaltic concrete core dams." *Hydropower and Dams 2009 World atlas industry guide*, Aqua-Media Int., UK.
- ICOLD. (1992). *Bituminous cores for fill dams*, Bulletin 84, International Commission on Large Dams (ICOLD), Paris.

- Kramer, R. W. (1988). "Embankment dams: Impervious elements other than clay cores." GR.Q61, *Transactions, 16th Int. Congress on Large Dams*, ICOLD Press, Paris, 1191–1253.
- Nakamura, Y., Okumura, T., Narita, K., and Ohne, Y. (2004). "Improvement of impervious asphalt mixture for high ductility against earthquake." *Proc., 4th Int. Conf. on Dam Engineering*, A.A. Balkema, Leiden, Netherlands, 18–20.
- Penman, A. D. M., and Charles, J. A. (1985). "A comparison between observed and predicted deformations of an embankment dam with a central asphaltic core." R.71-Q.56, *Transactions, 15th Int. Congress on Large Dams*, ICOLD Press, Paris, 1373–1389.
- Pircher, W., and Schwab, H. (1988). "Design, construction, and behavior of the asphaltic concrete core wall of the Finstertal Dam." R.49-Q.61, *Transactions, 16th Int. Congress on Large Dams*, ICOLD Press, Paris, 901–924.
- Saxegaard, H. (2002). "Asphalt core dams: Increased productivity to improve speed of construction." *Int. J. Hydropower Dams*, 9(6), 72–74.
- Schönian, E. (1999). *The Shell bitumen hydraulic engineering handbook*, Shell Int. Petroleum Co., London.
- Strobl, T., and Schmid, R. (1993). "The behavior of dams with asphaltic concrete cores during impounding." *Int. Water Power Dam Constr.*, 45(3), 29–34.
- Tschernutter, P. (1997). "Influence of soft rockfill material on a central bituminous concrete core membrane." *Proc., Non-Soil Water Barriers for Embankment Dams, 17th USCOLD Lecture Series*, U.S. Committee on Large Dams (USCOLD) Press, Denver, 57–68.
- Wang, W. (2008). "Research on the suitability of asphalt concrete as water barrier in dams and dikes." Ph.D. thesis, Dept. of Geosciences, University of Oslo, Norway.
- Wang, W., and Höeg, K. (2009). "Method of compaction has significant effects on stress-strain behavior of hydraulic asphalt concrete." *J. Test. Eval.*, 37(3), 264–274.